

# Proton Conduction in Zirconium-Based Metal–Organic Frameworks for Advanced Applications

Kai-Xin Zhao, Guo-Qin Zhang, Xin-Ru Wu, Hong-Bin Luo,\* Zhi-Xing Han, Yangyang Liu,\* and Xiao-Ming Ren

Cite This: *ACS Appl. Electron. Mater.* 2025, 7, 3164–3175

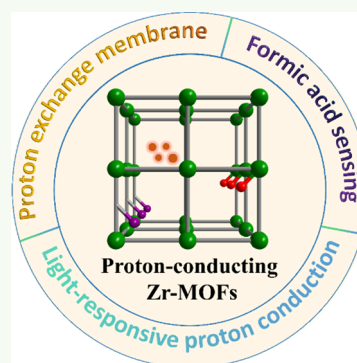
Read Online

ACCESS |

Metrics & More

Article Recommendations

**ABSTRACT:** Zirconium-based metal–organic frameworks (Zr-MOFs) have emerged as a promising class of crystalline porous materials, attracting significant interest in the field of proton conduction due to their exceptional chemical stability, structural flexibility, and functional tunability. Notably, proton-conducting Zr-MOFs show immense potential for diverse advanced technological applications. In this Spotlight on Applications paper, we provide an overview of proton-conducting Zr-MOFs and spotlight the recent progress of their utilization as proton exchange membranes in proton exchange membrane fuel cells (PEMFCs), light-responsive systems for proton pumps, and chemical sensors for formic acid detection. Furthermore, we also discussed the challenges, future prospects, and opportunities for promoting the application of proton-conducting Zr-MOFs.



**KEYWORDS:** Zr-MOFs, proton conduction, proton-exchange membrane, proton pumps, chemical sensor

## 1. INTRODUCTION

Proton conduction is a fundamental natural phenomenon, playing a critical role in various biochemical processes.<sup>1–5</sup> Notable examples include proton transport across the inner mitochondrial membrane<sup>6</sup> or chloroplast thylakoid membrane via ATP synthase,<sup>7</sup> and the proton-pumping mechanism of bacteriorhodopsin in halobacteria.<sup>8</sup> Beyond biological systems, solid-state proton-conducting materials have been developed to harness proton transport for numerous technological applications, such as fuel cells,<sup>9–11</sup> sensors,<sup>12–14</sup> electrolysis cells,<sup>15</sup> and electrochromic displays.<sup>16</sup> In these technologies, proton conductors function as solid electrolytes, selectively facilitating proton transport.

Conventional proton-conducting materials, including organic polymers,<sup>17,18</sup> ceramic oxides,<sup>19</sup> and solid acids,<sup>20</sup> have been extensively studied to elucidate their conduction mechanisms and optimize their performance for practical applications in electrochemical devices. Among them, Nafion is the most common and commercially available proton-conducting polymers. It consists of hydrophobic perfluorinated polyethylene backbones with pendant side chains terminating in hydrophilic sulfonic acid groups, conferring excellent structural integrity and hydrated proton conduction. Nafion exhibits proton conductivities of  $10^{-1}$ – $10^{-2}$  S·cm<sup>-1</sup> at moderate temperatures (60–80 °C) and high relative humidity (98% RH).<sup>21–24</sup> Despite their widespread use, Nafion faces significant limitations, including high production costs, environmentally hazardous manufacturing processes, and low

thermal stability.<sup>25,26</sup> Its proton conductivity heavily depends on water molecules, which act as proton carriers, resulting in a sharp decline in conductivity at temperatures above 80 °C.<sup>27,28</sup> Consequently, the search for alternative proton-conducting materials has gained significant attention from researchers in chemistry, physics, and materials science, driven by the growing demand for efficient and cost-effective solutions in electrochemical devices.

## 2. PROTON-CONDUCTING ZR-MOFS

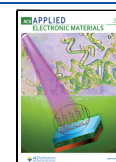
During the past decade, crystalline porous materials such as metal–organic frameworks (MOFs), covalent-organic frameworks (COFs), and hydrogen-bonded organic frameworks (HOFs) have been extensively studied for their potential as proton-conducting materials. Their well-defined crystalline structures enable direct observation of proton transport pathways and a deeper understanding of the associated mechanisms, shedding light on structure–function relationships. Among these, MOFs represent a versatile class of crystalline porous materials formed through the self-assembly

Received: January 24, 2025

Revised: March 12, 2025

Accepted: March 26, 2025

Published: April 3, 2025



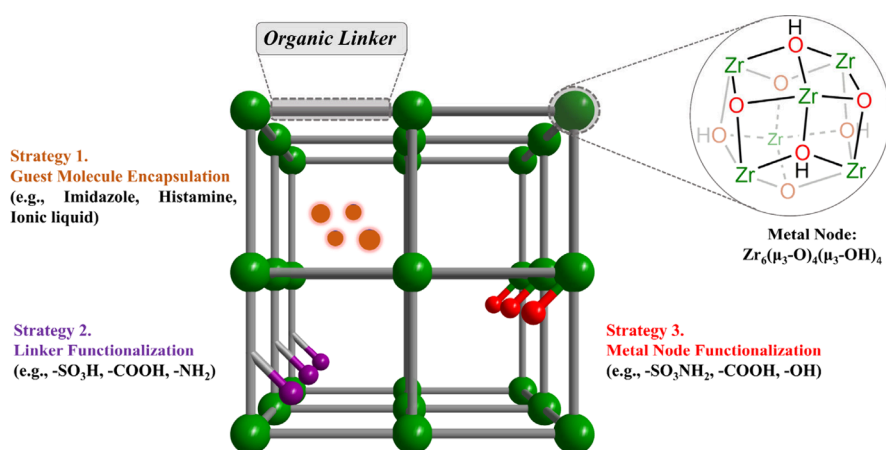


**Figure 1.** Schematic illustration of strategies for designing Zr-MOFs with proton conduction.

**Table 1.** Summary of Zr-MOF-Based Proton Conductors

MOFs	Conditions	$\sigma$ (S cm <sup>-1</sup> )	Ref
UiO-66	30 °C, 97% RH	$7.54 \times 10^{-6}$	63
UiO-66-NH <sub>2</sub>	30 °C, 97% RH	$1.4 \times 10^{-5}$	63
UiO-66-SO <sub>3</sub> H	30 °C, 97% RH	$3.4 \times 10^{-3}$	63
UiO-66-2COOH	30 °C, 97% RH	$1.0 \times 10^{-3}$	63
UiO-66(SH) <sub>2</sub>	80 °C, 90% RH	$2.25 \times 10^{-5}$	64
UiO-66(SO <sub>3</sub> H) <sub>2</sub>	80 °C, 90% RH	$8.4 \times 10^{-2}$	64
UiO-66-defects	65 °C, 95% RH	$6.93 \times 10^{-3}$	65
UiO-66-AS	80 °C, 98% RH	$1.7 \times 10^{-4}$	66
IM-UiO-66-AS	80 °C, 98% RH	$1.54 \times 10^{-1}$	66
PSM 1	80 °C, 95% RH	$1.64 \times 10^{-1}$	42
PSM 2	80 °C, 95% RH	$4.66 \times 10^{-3}$	42
Im@UiO-67	120 °C	$1.44 \times 10^{-3}$	67
IL@UiO-67	200 °C	$1.67 \times 10^{-3}$	68
MOF-801	25 °C, 98% RH	$1.88 \times 10^{-3}$	69
MIP-202(Zr)	90 °C, 95% RH	$1.1 \times 10^{-2}$	70
MOF-802	15 °C, 98% RH	$1.05 \times 10^{-2}$	71
Im@MOF-802-S	15 °C, 98% RH	$1.58 \times 10^{-2}$	71
MOF-808	42 °C, 99% RH	$7.58 \times 10^{-3}$	72
Im@MOF-808	65 °C, 98% RH	$3.45 \times 10^{-2}$	38
IL@UiO-66	70 °C, 98% RH	$1.42 \times 10^{-1}$	73
IL@MOF-808	70 °C, 98% RH	$7.01 \times 10^{-1}$	73
MOF-808-IL	60 °C, 100% RH	$1.28 \times 10^{-1}$	74
(Me <sub>2</sub> NH <sub>2</sub> ) <sub>4</sub> [Zr <sub>6</sub> (SO <sub>4</sub> ) <sub>6</sub> (μ <sub>3</sub> -O) <sub>3</sub> (HTHAM) <sub>3</sub> (CH <sub>3</sub> O) <sub>4</sub> ]·(DMF)·H <sub>2</sub> O	70 °C, 98% RH	$1.71 \times 10^{-1}$	75
[Zr <sub>18</sub> (SO <sub>4</sub> ) <sub>13</sub> (O/OH/H <sub>2</sub> O) <sub>56</sub> ]·xH <sub>2</sub> O	70 °C, 98% RH	$2.01 \times 10^{-2}$	75
Zr <sub>70</sub> (SO <sub>4</sub> ) <sub>58</sub> (O/OH) <sub>146</sub> ·x(H <sub>2</sub> O)·Mg(H <sub>2</sub> O) <sub>6</sub> ]	70 °C, 98% RH	$3.73 \times 10^{-2}$	75
60-UiO-66-1.8	100 °C, 98% RH	$3 \times 10^{-2}$	76
DUT-67(Zr)	100 °C, 98% RH	$2.98 \times 10^{-3}$	77
ZrP-3	90 °C, 95% RH	$1.91 \times 10^{-2}$	78
VNU-17	70 °C, 98% RH	$6.65 \times 10^{-6}$	79
HIm <sub>11</sub> CVNU-17	70 °C, 85% RH	$5.93 \times 10^{-3}$	79
VNU-23	70 °C, 90% RH	$2.5 \times 10^{-5}$	80
His <sub>8,2</sub> CVNU-23	95 °C, 85% RH	$1.79 \times 10^{-2}$	80
Zr <sub>6</sub> O <sub>4</sub> (OH) <sub>8</sub> L <sub>4,2</sub> ·xH <sub>2</sub> O	65 °C, 95% RH	$1.93 \times 10^{-3}$	58
AcOH@Zr <sub>6</sub> O <sub>4</sub> (OH) <sub>8</sub> L <sub>4</sub> ·xH <sub>2</sub> O	65 °C, 95% RH	$2.4 \times 10^{-3}$	58
SA@Zr <sub>6</sub> O <sub>4</sub> (OH) <sub>8</sub> L <sub>4</sub> ·xH <sub>2</sub> O	65 °C, 95% RH	$5.62 \times 10^{-3}$	58
H <sub>2</sub> SO <sub>4</sub> @Zr <sub>6</sub> O <sub>4</sub> (OH) <sub>8</sub> L <sub>3,8</sub> ·xH <sub>2</sub> O	65 °C, 95% RH	$3.46 \times 10^{-3}$	58
MOF-808-IMDC	80 °C, 98% RH	$1.11 \times 10^{-2}$	81
10HSA@MOF-808-(bSA) <sub>2</sub>	85 °C, 98% RH	$2.47 \times 10^{-1}$	82
MOF-808-4SA-150	60 °C, 95% RH	$7.89 \times 10^{-2}$	83
LiCl@UiO-66-F <sub>2</sub> (SO <sub>3</sub> H) <sub>2</sub>	90 °C, 90% RH	2.86	84

of metal ions or clusters with organic linkers. Their exceptional structural characteristics, including high crystallinity, porosity,

and tunable functionality, make them promising candidates for proton conduction.<sup>29–35</sup> The pores and channels of MOFs can

encapsulate guest proton carriers to enhance proton transport.<sup>36</sup> Alternatively, functionalizing the pore surfaces with specific groups can significantly boost proton conductivity.<sup>37,38</sup> The proton transfer process in MOFs is generally recognized to follow two primary mechanisms: the Grotthuss mechanism and the vehicle mechanism.<sup>39–41</sup> The Grotthuss mechanism involves a rapid proton-hopping process within an extended hydrogen-bonding network formed within the framework of MOFs, enabling efficient proton transport. In contrast, the vehicle mechanism relies on the diffusion of protonic species through the channels or pores of the MOFs. Notably, some MOF-based proton conductors achieved proton conductivities comparable to commercial Nafion.<sup>42,43</sup> Despite these advantages, MOFs face significant challenges, particularly their limited chemical stability under high humidity or acidic conditions.<sup>44,45</sup>

Among all MOFs, zirconium-based MOFs (Zr-MOFs) have garnered considerable attention due to their exceptional stability.<sup>46–49</sup> These materials feature  $Zr_6(\mu_3-O)_4(\mu_3-OH)_4$  clusters connected by multitopic carboxylate linkers.<sup>50,51</sup> Their superior chemical stability across a broad pH range and remarkable thermal robustness stem from the strong Zr(IV)–O coordination bonds within the clusters and between the nodes and carboxylate linkers.<sup>51</sup> Over the past decade, Zr-MOFs have been extensively explored in applications such as catalysis, molecular adsorption and separation, fluorescence sensing, drug delivery, and as porous carriers.<sup>52–57</sup> Additionally, both experimental and computational studies have demonstrated that the –OH groups on the  $Zr_6(\mu_3-O)_4(\mu_3-OH)_4$  clusters in Zr-MOFs possess low  $pK_a$  values,<sup>58</sup> allowing them to ionize readily and generate protons as charge carriers. This intrinsic property significantly enhances proton conductivity, making Zr-MOFs highly attractive for real-world applications in proton-conducting materials. As a result, Zr-MOFs have garnered considerable research interest in the field of proton conduction,<sup>59–62</sup> with ongoing efforts focused on optimizing their structural design and functionalization to further improve their performance in practical applications. To enhance the proton conductivity of Zr-MOFs, researchers have employed three primary strategies (Figure 1): (1) Guest Encapsulation: Incorporating guest molecules like imidazole, histamine, or ionic liquids as proton carriers within the Zr-MOF pores. (2) Linker Functionalization: Integrating acidic functional groups such as  $-SO_3H$ ,  $-COOH$ , or  $-NH_2$  into the Zr-MOF framework via linker modification. (3) Node Functionalization: Functionalizing  $Zr_6(\mu_3-O)_4(\mu_3-OH)_4$  clusters with moieties such as formate, sulfamate, or hydroxyl groups introduced during synthesis or post-synthetic treatment. These approaches have led to the development of numerous Zr-MOF-based proton conductors with impressive performance. A summary of representative examples is provided in Table 1, showing their potential for advancing proton-conducting materials.

### 3. APPLICATIONS

#### 3.1. Proton-Exchange Membrane Based on Zr-MOFs.

Proton exchange membrane fuel cells (PEMFCs) are advanced electrochemical devices that efficiently convert chemical energy into electrical energy with minimal environmental impact.<sup>85–87</sup> Their development is crucial for addressing global energy and environmental challenges. As the demand for clean, sustainable energy sources increases, PEMFCs stand out for their high energy conversion efficiency, zero pollutant emissions, and

versatility across diverse applications.<sup>88,89</sup> Central to PEMFC technology is the proton exchange membrane—the design and synthesis of a high-performance proton exchange membrane is critical to achieving optimal performance of PEMFCs.<sup>90–93</sup> To this date, Zr-MOFs have been extensively exploited for proton conduction,<sup>94–96</sup> however, Zr-MOFs are typically synthesized in powder form, which presents significant challenges for their direct application as proton exchange membranes in PEMFCs due to their poor processability.<sup>97,98</sup> Unlike conventional polymeric proton conductors, which can be readily fabricated into flexible and mechanically stable membranes, Zr-MOF powders lack the inherent mechanical integrity required for standalone membrane formation. As a result, they are not directly suitable for application in PEMFCs. The poor processability of Zr-MOFs in their powdered form remains a major barrier to their practical use in these fuel cell systems.<sup>17,99</sup> To solve this problem, Zr-MOF powders have been fabricated into composite membranes, which is considered a significant step toward their practical application in electrochemical devices.<sup>66,69,100–104</sup>

In 2017, we pioneered using MOF-808 for proton conduction, presenting the first example of proton-exchange membranes derived from this material.<sup>72</sup> MOF-808, a Zr-MOF composed of  $Zr_6(\mu_3-O)_4(\mu_3-OH)_4$  nodes connected by benzene tricarboxylate (BTC) linkers, forms a three-dimensional porous framework (Figure 2a). Under high relative humidity (98% RH), MOF-808 exhibited excellent room-temperature proton conductivity of  $2.14 \times 10^{-3} \text{ S}\cdot\text{cm}^{-1}$ , increasing to  $7.58 \times 10^{-3} \text{ S}\cdot\text{cm}^{-1}$  at 315 K. This performance is attributed to the ionization of terminal –COOH groups, which generate protons that migrate through hydrogen-bonding networks formed by adsorbed water molecules, –COOH,

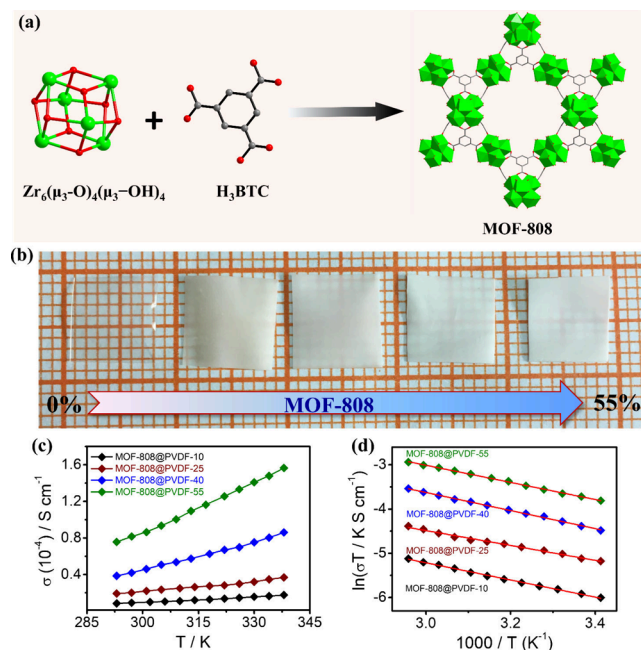


**Figure 2.** (a) Schematic illustrating the construction of MOF-808. (b) Optical images of the pure PVDF membrane and MOF-808@PVDF composite membranes. Reprinted with permission from ref 72. Copyright 2017 American Chemical Society. (c) Temperature-dependent proton conductivity and (d) the corresponding Arrhenius plots for MOF-808@PVDF composite membranes. Reprinted with permission from ref 72. Copyright 2017 American Chemical Society.

and  $\mu_3$ -OH groups. To enhance processability, we developed a series of composite membranes by incorporating MOF-808 microparticles into a poly(vinylidene fluoride) (PVDF) matrix. PVDF was selected for its excellent chemical and thermal stability, mechanical strength, and ease of membrane fabrication. MOF-808 particles were embedded into the PVDF matrix using a slurry casting method to create mixed-matrix membranes (MOF-808@PVDF-X, where X represents the mass percentage of MOF-808) (Figure 2b). These composite membranes combined the mechanical flexibility and durability of PVDF with the high proton conductivity of MOF-808. Proton conductivity tests revealed that the conductivity increased with both temperature and MOF-808 content. Among the samples, MOF-808@PVDF-55 demonstrated the highest performance, achieving proton conductivities of  $7.55 \times 10^{-5} \text{ S}\cdot\text{cm}^{-1}$  at 293 K and  $1.56 \times 10^{-4} \text{ S}\cdot\text{cm}^{-1}$  at 338 K (Figure 2c and 2d), making it suitable for PEMFC applications.

We further examined the proton-conducting properties of MOF-801, another Zr-MOF composed of  $\text{Zr}_6(\mu_3\text{-O})_4(\mu_3\text{-OH})_4$  nodes and fumarate linkers (Figure 3a).<sup>69</sup> MOF-801

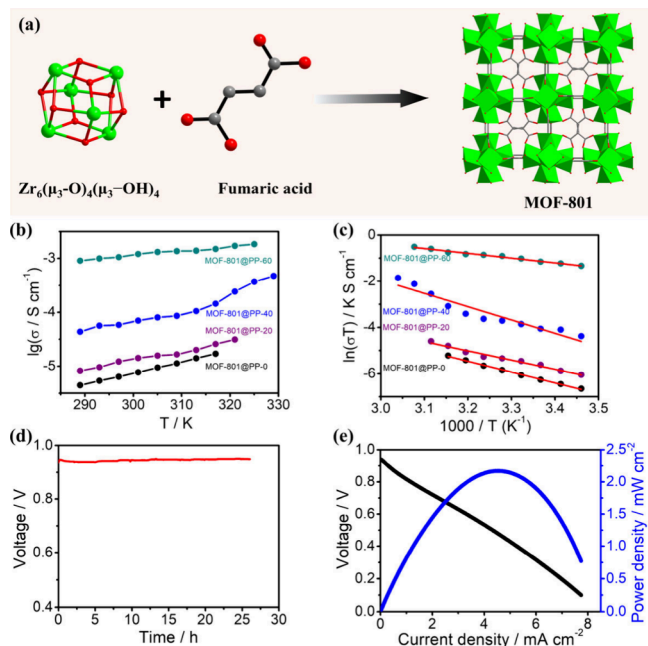


**Figure 3.** (a) Schematic illustrating the construction of MOF-801. (b) Temperature-dependent proton conductivity and (c) the corresponding Arrhenius plots for MOF-801@PP composite membranes. Reprinted with permission from ref 69. Copyright 2018 American Chemical Society. (d) The plot of open-circuit voltage versus time. (e) Polarization and power density curves of PEMFC prototype fabricated with MOF-801@PP-60 at 303 K and 100% RH. Reprinted with permission from ref 69. Copyright 2018 American Chemical Society.

exhibited excellent proton conductivity, reaching  $1.19 \times 10^{-3} \text{ S}\cdot\text{cm}^{-1}$  at 289 K and 98% RH, which increased further at higher temperatures, achieving  $4.16 \times 10^{-3} \text{ S}\cdot\text{cm}^{-1}$  at 334 K. The material also demonstrated exceptional chemical and water stability, retaining its structural integrity after exposure to boiling water, hydrochloric acid, and sodium hydroxide solutions. Building on these properties, we fabricated mixed-matrix membranes by combining MOF-801 microcrystals with a blend of poly(vinylpyrrolidone) (PVP) and PVDF. PVP, a

hydrophilic polymer, enhances the water-assisted proton transport within the composite membrane. Among these membranes, MOF-801@PP-60, with a 60% mass fraction of MOF-801, showed the highest proton conductivity of  $1.84 \times 10^{-3} \text{ S}\cdot\text{cm}^{-1}$  at 325 K and 98% RH (Figure 3b and 3c). When integrated into a PEMFC prototype, MOF-801@PP-60 delivered an open-circuit voltage of 0.95 V, a maximum power density of  $2.2 \text{ mW}\cdot\text{cm}^{-2}$  at  $4.53 \text{ mA}\cdot\text{cm}^{-2}$ , and demonstrated long-term stability (Figure 3d and 3e). These findings highlight the potential of Zr-MOFs as high-performance proton conductors for PEMFCs, providing new opportunities to advance clean energy technologies.

**3.2. Light-Responsive Proton Conduction of Zr-MOFs.** Biological proton pumps are integral membrane proteins that transport protons across membranes, creating a concentration gradient essential for various physiological processes.<sup>105,106</sup> Inspired by these natural systems, artificial stimuli-responsive proton-conducting materials have been developed to replicate their functionality.<sup>107–109</sup> These materials hold promise for applications in biomimetic processes such as ATP synthesis and power generation, as well as in bioelectronics and smart devices.<sup>109–113</sup> With growing interest in MOFs for proton conduction, stimuli-responsive proton-conducting MOFs have emerged as a focal point of research.<sup>38</sup> In 2017, Kitagawa et al. introduced the first optically switchable proton-conducting MOF by incorporating the photoactive molecule pyranine into melted  $[\text{Zn}(\text{HPO}_4)(\text{H}_2\text{PO}_4)_2](\text{ImH}_2)_2$ .<sup>114</sup> Subsequent efforts proposed grafting photoactive groups, such as azobenzene and spiropyran, onto MOF linkers to create light-responsive proton-conducting materials. Despite the versatility of Zr-MOFs as proton conductors, their light-responsive applications have received limited attention.

Recently, we demonstrated the first example of light-responsive proton conduction in Zr-MOFs.<sup>115</sup> Using a solvent-assisted ligand incorporation method, we substituted terminal formates on the  $\text{Zr}_6(\mu_3\text{-O})_4(\mu_3\text{-OH})_4$  nodes of MOF-808 with photoactive azobenzene-4,4'-dicarboxylic acid (AZOA), yielding MOF-808-AZOA (Figure 4a). The trans-cis isomerization of AZOA in MOF-808-AZOA is triggered by 365 nm UV light irradiation. As illustrated in Figure 4b, exposure to UV light causes the absorption peak at 340 nm, corresponding to the  $\pi$ - $\pi^*$  transition, to weaken rapidly within 50 s, while the absorption peak at 450 nm, associated with the  $n$ - $\pi^*$  transition, intensifies and undergoes a blue shift. In the absence of irradiation, AZOA predominantly exists in its trans-isomer form, and MOF-808-AZOA exhibits an ohmic resistance of approximately 15 k $\Omega$ . Under UV light, the trans-cis isomerization of AZOA leads to a significant increase in resistance, reaching an enhancement of about 200 times after 100 s, indicating a pronounced change in the proton conductivity of MOF-808-AZOA. When UV light is turned off, the AZOA gradually reverts to its trans-isomer state, accompanied by a decrease in resistance. Within 8 min, the resistance returns to its original value. During repeated cycles of UV light “ON” and “OFF”, MOF-808-AZOA demonstrates highly reversible and durable switchable resistance behavior (Figure 4c).

The isomerism of the AZOA ligand plays a crucial role in modulating the light-responsive proton conduction properties of Zr-MOFs. Structural simulations showed a clear difference in proton conductivity between the trans- and cis-configurations of AZOA. In the trans-configuration, the hydrogen

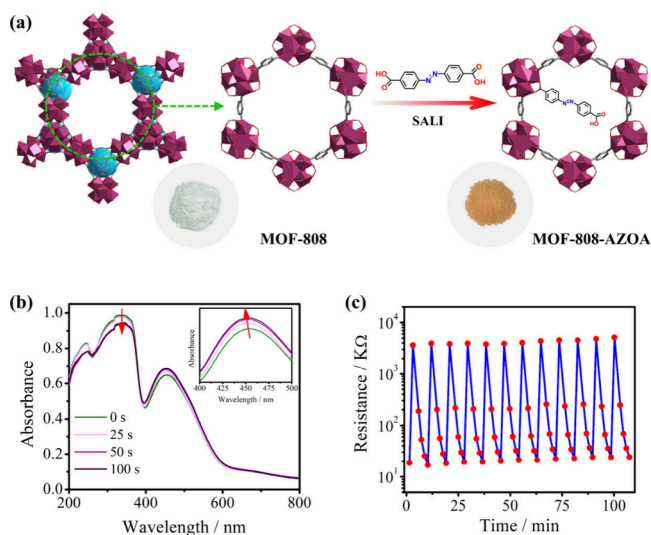


**Figure 4.** (a) Schematic illustration of the preparation of MOF-808-AZOA via solvent-assisted ligand incorporation (SALI). The inset shows the optical photographs of MOF-808 and MOF-808-AZOA. Reprinted with permission from ref 115. Copyright 2024 American Chemical Society. (b) Cycling impedance response of MOF-808-AZOA with and without 365 nm UV light irradiation. Reprinted with permission from ref 115. Copyright 2024 American Chemical Society. (c) Switchable resistance of MOF-808-AZOA with and without 365 nm UV light irradiation. Reprinted with permission from ref 115. Copyright 2024 American Chemical Society.

atom of the  $-\text{COOH}$  group and the oxygen atom of the terminal formates are 3.51 Å apart (Figure 5a). This distance

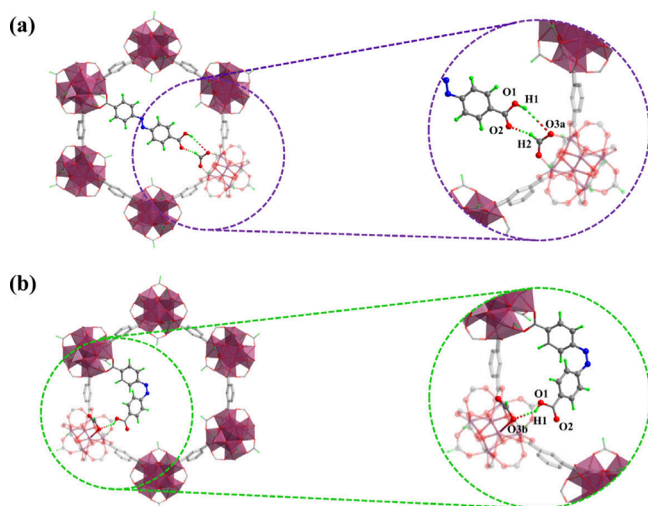


**Figure 5.** Molecular simulations on a single large pore structure of MOF-808 bearing an AZOA group in either the trans- (a) or cis- (b) configuration. The atoms are colored in plum (Zr), gray (C), red (O), blue (N), and green (H). Reprinted with permission from ref 115. Copyright 2024 American Chemical Society.

exceeds the combined van der Waals radii, preventing direct interaction between these groups. This separation also allows the hydrogen atom to ionize and transfer protons with the help of guest water molecules, promoting high proton conductivity. In contrast, the UV-induced cis-configuration brings the hydrogen and oxygen atoms into closer proximity (2.33 Å, Figure 5b), forming strong charge-assisted hydrogen bonds.

These bonds restrict the dissociation of the hydrogen atom from the  $-\text{COOH}$  group, suppressing proton conduction of the MOF. Therefore, the isomerization from the trans- to the cis-configuration of the AZOA ligand directly affects the proton conduction of the MOF. The trans-configuration allows proton dissociation and transfer, while the cis-configuration forms restrictive hydrogen bonds that impede proton movement. This example highlights the crucial role of ligand isomerism in tuning proton conductivity, offering potential for light-responsive applications where proton conduction can be controlled by switching ligand configurations.

Notably, by functionalizing the cluster nodes of MOF-808, the resulting MOF-808-AZOA exhibits a significantly shorter response time and a higher ON/OFF ratio in light-responsive proton conduction compared to MOFs functionalized through organic linkers, such as  $\text{Cu}_2(\text{F}_2\text{AzoBDC})_2(\text{dabco})^{111}$  and  $\text{Cu}_2(\text{SP-BPDC})_2(\text{dabco})^{116}$ . Furthermore, while MOF films incorporating photoactive species have demonstrated outstanding light-responsive proton conduction, their fabrication has been limited to Zn- or Cu-based MOFs due to the constraints imposed by the metal-hydroxide nanostrand confinement process.<sup>117–119</sup> In this context, the Zr-MOF cluster-node functionalization strategy introduced in our study presents a promising alternative. This approach not only could expand the applicability of light-responsive proton conduction to a broader range of MOFs but also could enhance their photoswitchable performance, overcoming the limitations of previously reported methods. However, the field is still in its early stages, facing challenges in achieving fast response times and high ON/OFF ratios. Developing effective strategies to expand the range of light-responsive proton-conducting Zr-MOFs and improve their performance represents a critical direction for future research.

**3.3. Formic Acid Sensing of Proton-Conducting Zr-MOFs.** Formic acid, a widely used organic compound in medicine, pesticides, rubber, and tannery industries, poses significant health and safety risks due to its high volatility and strong corrosivity.<sup>120–124</sup> The ease with which formic acid transitions into its gaseous form can lead to the corrosion of production equipment and pipelines, creating potential hazards in industrial environments.<sup>125–128</sup> Furthermore, human exposure to formic acid vapor can cause severe health issues, including dermatosis, bronchitis, chemical pneumonitis, and even fatality in extreme cases.<sup>124,129,130</sup> Consequently, the development of highly efficient sensors for formic acid vapor detection is of paramount importance, enabling effective air quality monitoring and timely detection of leaks to ensure both environmental and occupational safety.<sup>120,131–134</sup> MOFs have garnered significant attention as ideal sensing materials in electrochemical sensors due to their exceptional porosity, large surface area, and structural tunability/diversity.<sup>135–140</sup> These properties have enabled the detection of various gas molecules using MOFs, including ammonia,<sup>141</sup> nitrogen monoxide,<sup>142</sup> hydrogen sulfide,<sup>143</sup> and formaldehyde.<sup>144</sup> However, the development of MOF-based sensors for formic acid detection remains a significant challenge, primarily due to the chemical instability of most MOFs upon exposure to formic acid.<sup>145,146</sup> This instability leads to the collapse of their highly ordered crystal structures,<sup>134</sup> rendering them ineffective for such applications.

For the first time, we reported using crystalline thin films of proton-conducting Zr-MOFs for formic acid detection. MOF-802 was chosen for this application due to its intrinsic proton

conduction and exceptional chemical stability.<sup>146</sup> MOF-802, comprising  $Zr_6(\mu_3-O)_4(\mu_3-OH)_4$  cluster nodes and 1H-pyrazole-3,5-dicarboxylate (PZDC) linkers, maintains stability under harsh conditions, including in boiling water and acidic or basic aqueous environments. A crystalline thin film of MOF-802 was synthesized on a glass substrate using a solvothermal method, resulting in a densely packed and uniform structure. An interdigitated electrode was fabricated on the film to construct a custom sensor, which demonstrated excellent impedance response to formic acid (Figure 6a). The response-

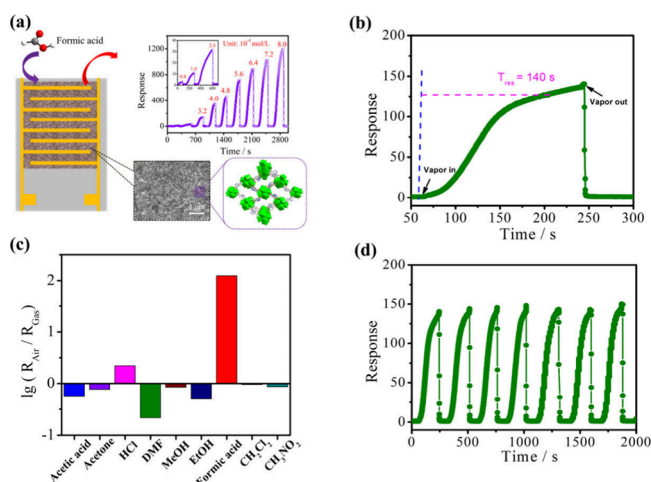


**Figure 6.** (a) Schematic illustration of MOF-802 thin film sensor for formic acid sensing. Reprinted with permission from ref 146. Copyright 2021 American Chemical Society. (b) Response–recovery time curve of MOF-802 thin film sensor toward  $3.2 \times 10^{-4}$  mol/L formic acid vapor. Reprinted with permission from ref 146. Copyright 2021 American Chemical Society. (c) Response of MOF-802 thin film sensor upon exposure to different chemical vapors. Reprinted with permission from ref 146. Copyright 2021 American Chemical Society. (d) Reproducibility cycles of MOF-802 thin film sensor toward  $3.2 \times 10^{-4}$  mol/L formic acid vapor. Reprinted with permission from ref 146. Copyright 2021 American Chemical Society.

recovery curve of the sensor for formic acid vapor at concentrations ranging from  $8.0 \times 10^{-5}$  to  $8.0 \times 10^{-4}$  mol/L shows a stepwise increase in response value with concentration. At  $3.2 \times 10^{-4}$  mol/L, the sensor exhibited a high response value of  $\sim 138$ , a short response time of  $\sim 140$  s, and achieved 90% of the maximum response (Figure 6b).

In MOF-802, besides the proton sources from  $Zr_6(\mu_3-O)_4(\mu_3-OH)_4$  nodes, two accessible Zr sites in each node are occupied by  $-COOH$  groups derived from formic acid used during synthesis. These  $-COOH$  groups also contribute to proton conduction. Upon exposure to formic acid vapor, molecules first adsorb onto the MOF-802 thin-film surface, then gradually permeate into the crystal channels. Permeation is slower than surface adsorption, as indicated by the rapid decrease in response after vapor removal. Thus, impedance changes mainly result from surface modifications. Adsorbed formic acid molecules promote proton transfer by forming hydrogen-bonding networks among their  $-COOH$  groups, the pyrazole nitrogen atoms of PZDC linkers, the  $-OH$  groups of  $Zr_6(\mu_3-O)_4(\mu_3-OH)_4$  nodes, and adsorbed water molecules. Higher vapor concentrations could increase adsorption, raising proton concentration and forming denser, more continuous hydrogen-bonding networks, significantly improving proton conductivity.

It is worth noting that MOF-802 thin-film sensors utilize different mechanisms from conventional metal-oxide semiconductor sensors for formic acid detection. While the latter relies on resistance changes due to shifts in the semiconductor's energy gap upon formic acid adsorption,<sup>120,147</sup> MOF-802 detects formic acid via its changes in proton conductivity. The sensing mechanism of the MOF-802 thin-film sensor also differs fundamentally from that of compacted pellets or interdigital electrodes composed of powdered crystalline MOFs used for chemical vapor detection. In MOF powder-based sensors, the response primarily stems from variations in grain-boundary resistance caused by the loose contact between crystalline grains. Several factors, such as the fabrication process of compacted pellets or interdigital electrodes and the size of crystalline grains, can significantly influence grain-boundary resistance. As a result, this type of impedance sensor often suffers from lower long-term stability, durability, and reproducibility.

On the other hand, the sensor based on MOF-802 demonstrated excellent repeatability, as evidenced by highly consistent response-recovery curves across test cycles and minimal degradation in response value and time during successive tests (Figure 6d). Furthermore, after four months of storage under ambient conditions, the sensor maintained its performance, confirming its long-term stability and reproducibility. In addition, the MOF-802-based sensor exhibited high selectivity for formic acid detection. As illustrated in Figure 6c, the sensor showed a slight response to HCl vapor, which was substantially lower than that for formic acid. In addition, the sensor showed negligible or opposite responses to other chemical vapors, including AcOH, MeOH, EtOH, Me<sub>2</sub>CO, DMF, MeNO<sub>2</sub>, and CH<sub>2</sub>Cl<sub>2</sub>, demonstrating its exceptional specificity for formic acid.

The potential of proton-conducting Zr-MOFs for highly efficient formic acid detection was further validated in our later study featuring MOF-801.<sup>148</sup> This Zr-MOF, composed of  $Zr_6(\mu_3-O)_4(\mu_3-OH)_4$  nodes and fumarate linkers, exhibits intrinsic proton conductivity and excellent chemical stability. The structural differences between MOF-801 and MOF-802 have a significant impact on their sensing performance for formic acid detection. MOF-801 possesses a more intricate pore architecture, featuring one octahedral cavity with a diameter of 7.4 Å and two crystallographically distinct tetrahedral cavities measuring 5.6 Å and 4.8 Å in diameter, respectively. This hierarchical pore structure results in a highly porous framework with a larger internal surface area, providing more active sites for molecular interactions and adsorption. In contrast, MOF-802 has a simpler pore structure, comprising only a single type of cavity with a uniform diameter of 5.6 Å, which inherently limits its porosity and available surface area for analyte adsorption. Due to its superior porosity and increased adsorption capacity, MOF-801 demonstrates significantly better sensing performance than MOF-802. The MOF-801 thin-film sensor exhibited outstanding sensitivity, selectivity, and durability for formic acid detection (Figures 7b and 7d), achieving a response magnitude of approximately 871 (Figure 7c), which was roughly six times higher than that of the MOF-802 thin-film sensor. This substantial difference can be attributed to the larger surface area of MOF-801 and more efficient molecular confinement, which facilitates stronger interactions with formic acid molecules. The hierarchical pore structure of MOF-801 may also enhance the diffusion and retention of formic acid analytes, further improving the

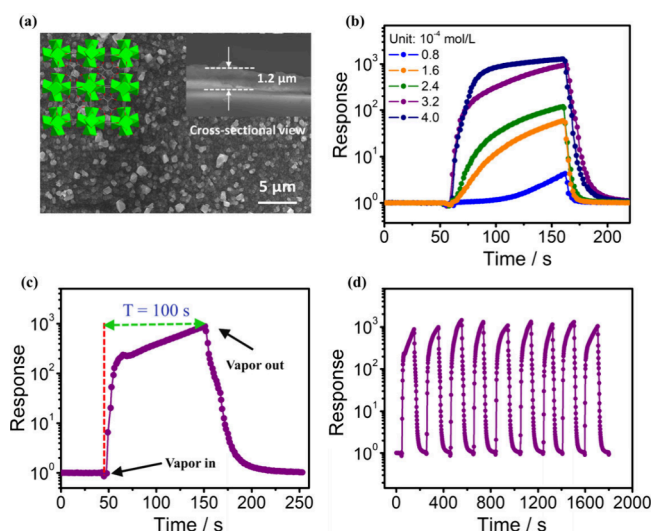


**Figure 7.** (a) SEM images of MOF-801 thin films. Reprinted with permission from ref 148. Copyright 2023 Elsevier. (b) Response of MOF-801 thin film sensor to formic acid with different concentrations. Reprinted with permission from ref 148. Copyright 2023 Elsevier. (c) Response–recovery time curve and (d) reproducibility cycles of MOF-801 thin film sensor to formic acid with a concentration of  $3.2 \times 10^{-4}$  mol/L. Reprinted with permission from ref 148. Copyright 2023 Elsevier.

sensor's response and stability. These findings highlight the crucial role of MOF topology in optimizing chemical sensing performance. Overall, these studies demonstrate the potential of proton-conducting Zr-MOF thin films as effective sensing materials for formic acid detection, offering promising opportunities for environmental and industrial applications.

#### 4. CONCLUSIONS AND OUTLOOK

In conclusion, zirconium-based metal–organic frameworks (Zr-MOFs) have emerged as a promising platform for developing next-generation proton-conducting materials due to their exceptional chemical stability, structural versatility, and functional tunability. Through strategies such as node functionalization, guest encapsulation, and linker modification, the proton conductivity of Zr-MOFs has been significantly enhanced, achieving levels comparable to commercial materials like Nafion. More importantly, proton-conducting Zr-MOFs hold great promise for various advanced applications, including use as proton exchange membranes in PEMFCs, stimuli-responsive proton conduction for proton pumps, and chemical sensors for gas detection.

Despite the significant progress made in this field, several challenges must be addressed to unlock the full potential of proton-conducting Zr-MOFs in practical applications. (i) Most Zr-MOFs are synthesized via solvothermal reactions, which are time-consuming and environmentally unfriendly due to their reliance on organic solvents. Hydrothermal conditions usually require high temperatures and pressures, complicating scalable production. Developing convenient, low-cost, and environmentally sustainable synthesis methods is crucial for facilitating the practical application of Zr-MOFs. (ii) Zr-MOFs are typically produced in powder form, which limits their direct application as proton exchange membranes in PEMFCs due to their poor processability. A viable solution involves combining Zr-MOFs with polymeric binders to create composite membranes. The compatibility between Zr-MOFs and

polymers significantly impacts the membranes' proton conductivity and mechanical properties. This issue may be addressed through surface modification of Zr-MOFs with organic functional groups to enhance interfacial compatibility. (iii) Research on stimuli-responsive proton conduction in Zr-MOFs remains in its infancy and warrants greater attention. Incorporating diverse functional groups into Zr-MOFs could improve performance, while exploring additional external stimuli could expand the range of applications. These efforts could open new avenues for the development of multifunctional proton-conducting materials. (iv) Compared to bulk pellets or composite membranes, Zr-MOF thin films offer significant advantages, including reduced crystal defects and an increased density of binding sites, making them ideal for chemical gas sensing. Reliable techniques for fabricating high-quality Zr-MOF thin films are needed to advance this application. Additionally, computational and theoretical studies can provide deeper insights into the sensing mechanisms of proton-conducting Zr-MOFs, particularly their interaction with specific analyte molecules.

Addressing these challenges will not only enhance the performance of proton-conducting Zr-MOFs but also broaden their scope of applications, paving the way for their integration into real-world technologies. Continued interdisciplinary research combining material synthesis, computational modeling, and device engineering is essential for advancing Zr-MOFs-based proton-conducting materials and their impactful contributions across diverse technological domains.

#### AUTHOR INFORMATION

##### Corresponding Authors

**Hong-Bin Luo** – State Key Laboratory of Materials-Oriented Chemical Engineering and College of Chemistry and Molecular Engineering, Nanjing Tech University, Nanjing 211816, P. R. China; [orcid.org/0000-0002-2225-7072](https://orcid.org/0000-0002-2225-7072); Email: [hbluo@njtech.edu.cn](mailto:hbluo@njtech.edu.cn)

**Yangyang Liu** – Department of Chemistry and Biochemistry, California State University, Los Angeles, Los Angeles, California 90032, United States; [orcid.org/0000-0002-3913-5979](https://orcid.org/0000-0002-3913-5979); Email: [yliu114@calstatela.edu](mailto:yliu114@calstatela.edu)

##### Authors

**Kai-Xin Zhao** – State Key Laboratory of Materials-Oriented Chemical Engineering and College of Chemistry and Molecular Engineering, Nanjing Tech University, Nanjing 211816, P. R. China

**Guo-Qin Zhang** – State Key Laboratory of Materials-Oriented Chemical Engineering and College of Chemistry and Molecular Engineering, Nanjing Tech University, Nanjing 211816, P. R. China; [orcid.org/0000-0002-9080-1324](https://orcid.org/0000-0002-9080-1324)

**Xin-Ru Wu** – State Key Laboratory of Materials-Oriented Chemical Engineering and College of Chemistry and Molecular Engineering, Nanjing Tech University, Nanjing 211816, P. R. China

**Zhi-Xing Han** – State Key Laboratory of Materials-Oriented Chemical Engineering and College of Chemistry and Molecular Engineering, Nanjing Tech University, Nanjing 211816, P. R. China

**Xiao-Ming Ren** – State Key Laboratory of Materials-Oriented Chemical Engineering and College of Chemistry and Molecular Engineering, Nanjing Tech University, Nanjing 211816, P. R. China; State Key Laboratory of Coordination

Chemistry, Nanjing University, Nanjing 210023, P. R. China; [orcid.org/0000-0003-0848-6503](https://orcid.org/0000-0003-0848-6503)

Complete contact information is available at:  
<https://pubs.acs.org/10.1021/acsaelm.5c00183>

## Notes

The authors declare no competing financial interest.

## ACKNOWLEDGMENTS

This work is financially supported by the National Natural Science Foundation of China (Grant Nos 22073047 and 22101131), Natural Science Foundation of Jiangsu Province (Grant No. BK20210543), and the Priority Academic Program Development of Jiangsu Higher Education Institutions. Y.L. also acknowledges the financial support from NSF PREM (Grant No. DMR 2425229).

## REFERENCES

- (1) Wang, S. B.; Luo, H. L.; Li, X.; Shi, L.; Cheng, B. W.; Zhuang, X. P.; Li, Z. H. Amino Acid-Functionalized Metal Organic Framework with Excellent Proton Conductivity for Proton Exchange Membranes. *Int. J. Hydrogen Energy* **2021**, *46*, 1163–1173.
- (2) Xiang, Y.; Zhang, J.; Liu, Y.; Guo, Z. B.; Lu, S. F. Design of an Effective Methanol-Blocking Membrane with Purple Membrane for Direct Methanol Fuel Cells. *J. Membr. Sci.* **2011**, *367*, 325–331.
- (3) Amdursky, N.; Wang, X. H.; Meredith, P.; Bradley, D. D. C.; Stevens, M. M. Long-Range Proton Conduction across Free-Standing Serum Albumin Mats. *Adv. Mater.* **2016**, *28*, 2692–2698.
- (4) Ho, D.; Chu, B.; Lee, H.; Montemagno, C. D. Protein-Driven Energy Transduction across Polymeric Biomembranes. *Nanotechnology* **2004**, *15*, 1084–1094.
- (5) Ramanthrikkovil Variyam, A.; Stolov, M.; Feng, J. J.; Amdursky, N. Solid-State Molecular Protonics Devices of Solid-Supported Biological Membranes Reveal the Mechanism of Long-Range Lateral Proton Transport. *ACS Nano* **2024**, *18*, 5101–5112.
- (6) Wagner, K.; Mick, D. U.; Rehling, P. Protein Transport Machineries for Precursor Translocation across the Inner Mitochondrial Membrane. *Biochim. Biophys. Acta, Mol. Cell Res.* **2009**, *1793*, 52–59.
- (7) Correa Galvis, V.; Strand, D. D.; Messer, M.; Thiele, W.; Bethmann, S.; Hübner, D.; Uflewski, M.; Kaiser, E.; Siemiatkowska, B.; Morris, B. A.; Tóth, S. Z.; Watanabe, M.; Brückner, F.; Höfgen, R.; Jahns, P.; Schöttler, M. A.; Armbruster, U. H<sup>+</sup> Transport by K<sup>+</sup> Exchange Antporter3 Promotes Photosynthesis and Growth in Chloroplast Atp Synthase Mutants. *Plant Physiol.* **2020**, *182*, 2126–2142.
- (8) Ramirez, F.; Okazaki, H.; Tu, S. I. Effects of Phospholipid Composition on Activities of Bacteriorhodopsin in Reconstituted Purple Membrane. *FEBS Lett.* **1981**, *135*, 123–126.
- (9) Benhabbour, S. R.; Chapman, R. P.; Scharfenberger, G.; Meyer, W. H.; Goward, G. R. Study of Imidazole-Based Proton-Conducting Composite Materials Using Solid-State Nmr. *Chem. Mater.* **2005**, *17*, 1605–1612.
- (10) Wang, B.; Bi, L.; Zhao, X. S. Liquid-Phase Synthesis of SrCo<sub>0.9</sub>Nb<sub>0.1</sub>O<sub>3-δ</sub> Cathode Material for Proton-Conducting Solid Oxide Fuel Cells. *Ceram. Int.* **2018**, *44*, 5139–5144.
- (11) Luo, H. B.; Ren, L. T.; Ning, W. H.; Liu, S. X.; Liu, J. L.; Ren, X. M. Robust Crystalline Hybrid Solid with Multiple Channels Showing High Anhydrous Proton Conductivity and a Wide Performance Temperature Range. *Adv. Mater.* **2016**, *28*, 1663–1667.
- (12) Hinojo, A.; Lujan, E.; Verdager, A.; Colominas, S.; Abella, J. Zn Sintering Aid Effect on Proton Conductivity of BaCe<sub>0.4</sub>Zr<sub>0.3</sub>Y<sub>0.1</sub>O<sub>3-Δ</sub> Electrolyte for Hydrogen Sensors. *Ceram. Int.* **2024**, *50*, 40205–40215.
- (13) Kalyakin, A.; Volkov, A.; Lyagaeva, J.; Medvedev, D.; Demin, A.; Tsiakaras, P. Combined Amperometric and Potentiometric Hydrogen Sensors Based on BaCe<sub>0.7</sub>Zr<sub>0.1</sub>Y<sub>0.2</sub>O<sub>3-Δ</sub> Proton-Conducting Ceramic. *Sens. Actuators, B* **2016**, *231*, 175–182.
- (14) Zhang, J.; Zhang, R.; Liu, Y. Y.; Kong, Y. R.; Luo, H. B.; Zou, Y.; Zhai, L.; Ren, X. M. Acidic Groups Functionalized Carbon Dots Capping Channels of a Proton Conductive Metal–Organic Framework by Coordination Bonds to Improve the Water-Retention Capacity and Boost Proton Conduction. *ACS Appl. Mater. Interfaces* **2021**, *13*, 60084–60091.
- (15) Leng, Z. Z.; Huang, Z. Z.; Zhou, X.; Zhang, B.; Bai, H.; Zhou, J.; Wang, S. R. The Effect of Sintering Aids on BaCe<sub>0.7</sub>Zr<sub>0.1</sub>Y<sub>0.1</sub>Yb<sub>0.1</sub>O<sub>3-Δ</sub> as the Electrolyte of Proton-Conducting Solid Oxide Electrolysis Cells. *Int. J. Hydrogen Energy* **2022**, *47*, 33861–33871.
- (16) Gu, C.; Jia, A. B.; Zhang, Y. M.; Zhang, S. X. A. Emerging Electrochromic Materials and Devices for Future Displays. *Chem. Rev.* **2022**, *122*, 14679–14721.
- (17) Mauritz, K. A.; Moore, R. B. State of Understanding of Nafion. *Chem. Rev.* **2004**, *104*, 4535–4586.
- (18) Kreuer, K. D. On the Development of Proton Conducting Polymer Membranes for Hydrogen and Methanol Fuel Cells. *J. Membr. Sci.* **2001**, *185*, 29–39.
- (19) Norby, T.; Friesel, M.; Mallander, B. E. Proton and Deuteron Conductivity in CsHSO<sub>4</sub> and CsDSO<sub>4</sub> by in Situ Isotopic Exchange. *Solid State Ionics* **1995**, *77*, 105–110.
- (20) Lu, Y. F.; Yang, Y.; Sellinger, A.; Lu, M. C.; Huang, J. M.; Fan, H. Y.; Haddad, R.; Lopez, G.; Burns, A. R.; Sasaki, D. Y.; Shelnutt, J.; Brinker, C. J. Self-Assembly of Mesoscopically Ordered Chromatic Polydiacetylene/Silica Nanocomposites. *Nature* **2001**, *410*, 913–917.
- (21) Alberti, G.; Casciola, M. Solid State Protonic Conductors, Present Main Applications and Future Prospects. *Solid State Ionics* **2001**, *145*, 3–16.
- (22) Peighambaroust, S. J.; Rowshanzamir, S.; Amjadi, M. Review of the Proton Exchange Membranes for Fuel Cell Applications. *Int. J. Hydrogen Energy* **2010**, *35*, 9349–9384.
- (23) Ochi, S.; Kamishima, O.; Mizusaki, J.; Kawamura, J. Investigation of Proton Diffusion in Nafion®117 Membrane by Electrical Conductivity and Nmr. *Solid State Ionics* **2009**, *180*, 580–584.
- (24) Karimi, M. B.; Mohammadi, F.; Hooshyari, K. Recent Approaches to Improve Nafion Performance for Fuel Cell Applications: A Review. *Int. J. Hydrogen Energy* **2019**, *44*, 28919–28938.
- (25) Hernández-Flores, G.; Poggi-Valardo, H. M.; Solorza-Feria, O. Comparison of Alternative Membranes to Replace High Cost Nafion Ones in Microbial Fuel Cells. *Int. J. Hydrogen Energy* **2016**, *41*, 23354–23362.
- (26) Koók, L.; Kaufer, B.; Bakonyi, P.; Rózsenszki, T.; Rivera, I.; Buitrón, G.; Bélafi-Bakó, K.; Nemestóthy, N. Supported Ionic Liquid Membrane Based on [BMIM][PF<sub>6</sub>] Can Be a Promising Separator to Replace Nafion in Microbial Fuel Cells and Improve Energy Recovery: A Comparative Process Evaluation. *J. Membr. Sci.* **2019**, *570–571*, 215–225.
- (27) Barique, M. A.; Tsuchida, E.; Ohira, A.; Tashiro, K. Effect of Elevated Temperatures on the States of Water and Their Correlation with the Proton Conductivity of Nafion. *ACS Omega* **2018**, *3*, 349–360.
- (28) Meng, Z. Y.; Zou, Y. X.; Li, N. N.; Wang, B.; Fu, X. D.; Zhang, R.; Hu, S. F.; Bao, X. J.; Li, X.; Zhao, F.; Liu, Q. T. Graphene Oxide-Intercalated Microbial Montmorillonite to Moderate the Dependence of Nafion-Based Pemfcs in High-Humidity Environments. *ACS Appl. Mater. Interfaces* **2023**, *6*, 1771–1780.
- (29) Li, X.; Shu, X. Y.; Shi, Y. X.; Li, H. L.; Pei, X. B. MOFs and Bone: Application of MOFs in Bone Tissue Engineering and Bone Diseases. *Chin. Chem. Lett.* **2023**, *34*, 107986.
- (30) Zhu, W. J.; Zhao, J. Y.; Chen, Q.; Liu, Z. Nanoscale Metal–Organic Frameworks and Coordination Polymers as Theranostic Platforms for Cancer Treatment. *Coord. Chem. Rev.* **2019**, *398*, 113009.
- (31) Kim, J. Y.; Balderas Xicohtencatl, R.; Zhang, L. D.; Kang, S. G.; Hirscher, M.; Oh, H.; Moon, H. R. Exploiting Diffusion Barrier and

Chemical Affinity of Metal–Organic Frameworks for Efficient Hydrogen Isotope Separation. *J. Am. Chem. Soc.* **2017**, *139*, 15135–15141.

(32) Simon-Yarza, T.; Mielcarek, A.; Couvreur, P.; Serre, C. Nanoparticles of Metal–Organic Frameworks: On the Road to in Vivo Efficacy in Biomedicine. *Adv. Mater.* **2018**, *30*, 1707365.

(33) Cai, M. R.; Chen, G. S.; Qin, L. Y.; Qu, C. H.; Dong, X. X.; Ni, J.; Yin, X. B. Metal Organic Frameworks as Drug Targeting Delivery Vehicles in the Treatment of Cancer. *Pharmaceutics* **2020**, *12*, 232.

(34) Zhang, J.; He, X.; Kong, Y. R.; Luo, H. B.; Liu, M.; Liu, Y. Y.; Ren, X. M. Efficiently Boosting Moisture Retention Capacity of Porous Superprotonic Conducting MOF-802 at Ambient Humidity Via Forming a Hydrogel Composite Strategy. *ACS Appl. Mater. Interfaces* **2021**, *13*, 37231–37238.

(35) Luo, H. B.; Lin, F. R.; Liu, Z. Y.; Kong, Y. R.; Idrees, K. B.; Liu, Y. Y.; Zou, Y.; Farha, O. K.; Ren, X. M. MOF–Polymer Mixed Matrix Membranes as Chemical Protective Layers for Solid-Phase Detoxification of Toxic Organophosphates. *ACS Appl. Mater. Interfaces* **2023**, *15*, 2933–2939.

(36) Sharma, A.; Lim, J.; Lah, M. S. Strategies for Designing Metal–Organic Frameworks with Superprotonic Conductivity. *Coord. Chem. Rev.* **2023**, *479*, 214995.

(37) Li, X. M.; Jia, J. C.; Yang, D. T.; Jin, J. L.; Gao, J. K. Construction of Biomimetic Proton Transport Channels in Metal–Organic Framework. *Chin. Chem. Lett.* **2024**, *35*, 108474.

(38) Luo, H. B.; Ren, Q.; Wang, P.; Zhang, J.; Wang, L. F.; Ren, X. M. High Proton Conductivity Achieved by Encapsulation of Imidazole Molecules into Proton-Conducting MOF-808. *ACS Appl. Mater. Interfaces* **2019**, *11*, 9164–9171.

(39) Pal, S. C.; Das, M. C. Superprotonic Conductivity of MOFs and Other Crystalline Platforms Beyond  $10^{-1}$  S cm $^{-1}$ . *Adv. Funct. Mater.* **2021**, *31*, 2101584.

(40) Ramaswamy, P.; Wong, N. E.; Shimizu, G. K. H. MOFs as Proton Conductors—Challenges and Opportunities. *Chem. Soc. Rev.* **2014**, *43*, 5913–5932.

(41) Lim, D.-W.; Kitagawa, H. Proton Transport in Metal–Organic Frameworks. *Chem. Rev.* **2020**, *120*, 8416–8467.

(42) Mukhopadhyay, S.; Debgupta, J.; Singh, C.; Sarkar, R.; Basu, O.; Das, S. K. Designing UiO-66-Based Superprotonic Conductor with the Highest Metal–Organic Framework Based Proton Conductivity. *ACS Appl. Mater. Interfaces* **2019**, *11*, 13423–13432.

(43) Zhang, Z. C.; Liang, L. X.; Feng, J. Z.; Hou, G. J.; Ren, W. C. Significant Enhancement of Proton Conductivity in Solid Acid at the Monolayer Limit. *Nat. Commun.* **2024**, *15*, 2706.

(44) Lu, Y. B.; Liao, Y. Q.; Dong, L.; Zhu, S. D.; Wen, H. R.; Huang, J.; Dai, X. X.; Lian, P.; Jiang, X. M.; Li, R.; Xie, Y. R. Ultra-Stable Metal–Organic Framework with Concurrent High Proton Conductivity and Fluorescence Sensing for Nitrobenzene. *Chem. Mater.* **2021**, *33*, 7858–7868.

(45) He, T.; Kong, X. J.; Zhou, J.; Zhao, C.; Wang, K. C.; Wu, X. Q.; Lv, X. L.; Si, G. R.; Li, J. R.; Nie, Z. R. A Practice of Reticular Chemistry: Construction of a Robust Mesoporous Palladium Metal–Organic Framework Via Metal Metathesis. *J. Am. Chem. Soc.* **2021**, *143*, 9901–9911.

(46) Sha, F. R.; Wang, X. L.; Kirlikovali, K. O.; Farha, O. K. Enhancing Biocatalysis: Metal–Organic Frameworks as Multifunctional Enzyme Hosts. *Acc. Chem. Res.* **2024**, *57*, 3500–3511.

(47) Taddei, M. When Defects Turn into Virtues: The Curious Case of Zirconium-Based Metal–Organic Frameworks. *Coord. Chem. Rev.* **2017**, *343*, 1–24.

(48) Panda, S.; Kundu, S.; Malik, P.; Haldar, R. Leveraging Metal Node-Linker Self-Assembly to Access Functional Anisotropy of Zirconium-Based MOF-on-MOF Epitaxial Heterostructure Thin Films. *Chem. Sci.* **2024**, *15*, 2586–2592.

(49) Chen, Y. W.; Xie, H. M.; Zhong, Y. H.; Sha, F. R.; Kirlikovali, K. O.; Wang, X. L.; Zhang, C. H.; Li, Z. B.; Farha, O. K. Programmable Water Sorption through Linker Installation into a Zirconium Metal–Organic Framework. *J. Am. Chem. Soc.* **2024**, *146*, 11202–11210.

(50) Chen, Z. J.; Hanna, S. L.; Redfern, L. R.; Alezi, D.; Islamoglu, T.; Farha, O. K. Reticular Chemistry in the Rational Synthesis of Functional Zirconium Cluster-Based MOFs. *Coord. Chem. Rev.* **2019**, *386*, 32–49.

(51) Howarth, A. J.; Liu, Y. Y.; Li, P.; Li, Z. Y.; Wang, T. C.; Hupp, J. T. Chemical, Thermal and Mechanical Stabilities of Metal–Organic Frameworks. *Nat. Rev. Mater.* **2016**, *1*, 15018.

(52) Daliran, S.; Oveisi, A. R.; Kung, C.-W.; Sen, U.; Dhakshinamoorthy, A.; Chuang, C.-H.; Khajeh, M.; Erkartal, M.; Hupp, J. T. Defect-Enabling Zirconium-Based Metal–Organic Frameworks for Energy and Environmental Remediation Applications. *Chem. Soc. Rev.* **2024**, *53*, 6244–6294.

(53) Majewski, M. B.; Howarth, A. J.; Li, P.; Wasielewski, M. R.; Hupp, J. T.; Farha, O. K. Enzyme Encapsulation in Metal–Organic Frameworks for Applications in Catalysis. *CrystEngComm* **2017**, *19*, 4082–4091.

(54) Shi, L.; Kirlikovali, K. O.; Chen, Z. J.; Farha, O. K. Metal–Organic Frameworks for Water Vapor Adsorption. *Chem.* **2024**, *10*, 484–503.

(55) Han, Z. X.; Cai, W. J.; Lin, F. R.; Zhao, K. X.; Luo, H. B.; Liu, Z. Y.; Liu, Y. Y.; Liu, J. L.; Ren, X. M. Integrating Metal–Organic Framework Particles on Fabric Membranes for Decontaminating Toxic Organophosphates. *Microporous Mesoporous Mater.* **2024**, *375*, 113175.

(56) Luo, H. B.; Castro, A. J.; Wasson, M. C.; Flores, W.; Farha, O. K.; Liu, Y. Y. Rapid, Biomimetic Degradation of a Nerve Agent Simulant by Incorporating Imidazole Bases into a Metal–Organic Framework. *ACS Catal.* **2021**, *11*, 1424–1429.

(57) Gao, J. L.; Zhao, X. L.; Ni, X. Q.; Mo, Y. H.; Tong, Y. B.; Cao, D. Q.; Luo, H. B.; Qiao, Q.; Ren, X. M. Multicomponent Quasi-Solid-State Polymer Electrolyte Incorporating MOFs and Halloysite Nanotubes for Enhanced Sodium Metal Battery Performance. *ACS Appl. Energy Mater.* **2024**, *7*, 10196–10202.

(58) Taylor, J. M.; Komatsu, T.; Dekura, S.; Otsubo, K.; Takata, M.; Kitagawa, H. The Role of a Three Dimensionally Ordered Defect Sublattice on the Acidity of a Sulfonated Metal–Organic Framework. *J. Am. Chem. Soc.* **2015**, *137*, 11498–11506.

(59) Mukherjee, D.; Pal, S. C.; Oruganti, Y.; Lee, B. G.; Manna, A. K.; Lim, D.-W.; Das, M. C. Intermediate Temperature Superprotonic Conductivity Beyond  $10^{-2}$  S cm $^{-1}$  with Low Proton Transfer Energy Barrier in a Metal–Organic Framework. *ACS Energy Lett.* **2025**, *10*, 1216–1228.

(60) Li, X.-M.; Jia, J.; Liu, D.; Xiao, M.; Xu, L. Directed Regulation of Proton Transport Pathways in MOF-808. *Inorg. Chem.* **2025**, *64*, 5196.

(61) Yang, C.; Liu, Y.; Li, J.; Zhuang, S.; Wang, F.; Lin, Z.; Zhao, Y.; Huang, W. Linkage Position-Controlled Synthesis of Diverse Zirconium Metal–Organic Frameworks with Prominent Intrinsic Proton Conductivities. *Inorg. Chem.* **2025**, *64*, 5271.

(62) Kang, I.; Lee, S.; Choi, W.-J.; Lee, S.; So, S.; Yu, D. M.; Yoon, S. J.; Kim, D.-W.; Nam, K. W.; Oh, K.-H. Effect of Metal–Organic Framework on Hydrogen Volume Fraction in the Oxygen-Rich Anode Catalyst Layer of Proton Exchange Membrane Water Electrolyzer. *Chem. Eng. J.* **2025**, *508*, 161094.

(63) Yang, F.; Huang, H. L.; Wang, X. Y.; Li, F.; Gong, Y. H.; Zhong, C. L.; Li, J. R. Proton Conductivities in Functionalized UiO-66: Tuned Properties, Thermogravimetry Mass, and Molecular Simulation Analyses. *Cryst. Growth Des.* **2015**, *15*, 5827–5833.

(64) Phang, W. J.; Jo, H.; Lee, W. R.; Song, J. H.; Yoo, K.; Kim, B.; Hong, C. S. Superprotonic Conductivity of a UiO-66 Framework Functionalized with Sulfonic Acid Groups by Facile Postsynthetic Oxidation. *Angew. Chem., Int. Ed.* **2015**, *54*, 5142–5146.

(65) Taylor, J. M.; Dekura, S.; Ikeda, R.; Kitagawa, H. Defect Control to Enhance Proton Conductivity in a Metal–Organic Framework. *Chem. Mater.* **2015**, *27*, 2286–2289.

(66) Li, X. M.; Liu, J.; Zhao, C.; Zhou, J. L.; Zhao, L.; Li, S. L.; Lan, Y. Q. Strategic Hierarchical Improvement of Superprotonic Conductivity in a Stable Metal–Organic Framework System. *J. Mater. Chem. A* **2019**, *7*, 25165–25171.

- (67) Liu, S. C.; Yue, Z. F.; Liu, Y. Incorporation of Imidazole within the Metal-Organic Framework UiO-67 for Enhanced Anhydrous Proton Conductivity. *Dalton Trans.* **2015**, *44*, 12976–12980.
- (68) Chen, L. H.; Wu, B. B.; Zhao, H. X.; Long, L. S.; Zheng, L. S. High Temperature Ionic Conduction Mediated by Ionic Liquid Incorporated within the Metal-Organic Framework UiO-67(Zr). *Inorg. Chem. Commun.* **2017**, *81*, 1–4.
- (69) Zhang, J.; Bai, H. J.; Ren, Q.; Luo, H. B.; Ren, X. M.; Tian, Z. F.; Lu, S. F. Extra Water- and Acid-Stable MOF-801 with High Proton Conductivity and Its Composite Membrane for Proton-Exchange Membrane. *ACS Appl. Mater. Interfaces* **2018**, *10*, 28656–28663.
- (70) Wang, S. J.; Wahiduzzaman, M.; Davis, L.; Tissot, A.; Shepard, W.; Marrot, J.; Martineau-Corcus, C.; Hamdane, D.; Maurin, G.; Devautour-Vinot, S.; Serre, C. A Robust Zirconium Amino Acid Metal-Organic Framework for Proton Conduction. *Nat. Commun.* **2018**, *9*, 4937.
- (71) Lin, F. R.; Liu, Z. Y.; Zhang, G. Q.; Zhang, J.; Ren, X. M. Understanding Proton Conduction Enhancement of MOF-802 through in Situ Incorporation of Imidazole into Its Channels. *Inorg. Chem. Commun.* **2023**, *157*, 111340.
- (72) Luo, H. B.; Wang, M.; Liu, S. X.; Xue, C.; Tian, Z. F.; Zou, Y.; Ren, X. M. Proton Conductance of a Superior Water-Stable Metal-Organic Framework and Its Composite Membrane with Poly-(Vinylidene Fluoride). *Inorg. Chem.* **2017**, *56*, 4169–4175.
- (73) Li, X. M.; Wang, Y. M.; Wu, B.; Zeng, L. Efficient Proton Transport in Stable Functionalized Channels of Zirconium Metal-Organic Frameworks. *ACS Appl. Energy Mater.* **2021**, *4*, 8303–8310.
- (74) Jia, J. J.; Li, X. M.; Wu, H.; Huang, Q.; Gao, J. K. Achieving High Intrinsic Proton Conductivity Via Functionalization of MOF-808 by Ionic Liquid. *ACS Sustainable Chem. Eng.* **2023**, *11*, 13502–13507.
- (75) Xie, W. L.; Li, X. M.; Lin, J. M.; Dong, L. Z.; Chen, Y.; Li, N.; Shi, J. W.; Liu, J.; et al. i.; Liu, J.; Li, S. L.; Lan, Y. Q. Keeping Superprotonic Conductivity over a Wide Temperature Region Via Sulfate Hopping Sites-Decorated Zirconium-Oxo Clusters. *Small* **2022**, *18*, 2205444.
- (76) Liu, Q. Q.; Liu, S. S.; Liu, X. F.; Xu, X. J.; Dong, X. Y.; Zhang, H. J.; Zang, S. Q. Superprotonic Conductivity of UiO-66 with Missing-Linker Defects in Aqua-Ammonia Vapor. *Inorg. Chem.* **2022**, *61*, 3406–3411.
- (77) Kang, L. L.; Xing, C.; Jin, Y. X.; Xie, L. X.; Li, Z. F.; Li, G. Two Dual-Function Zr/Hf-MOFs as High-Performance Proton Conductors and Amines Impedance Sensors. *Inorg. Chem.* **2023**, *62*, 3036–3046.
- (78) Gui, D. X.; Zhang, J. e.; Wang, X. Y.; Wang, C. Z.; Wang, Q.; Zhang, Y. G.; Li, H.; Wang, S. A. Ionothermal Synthesis of a Highly Crystalline Zirconium Phosphate Proton Conductor. *Dalton Trans.* **2022**, *51*, 8182–8185.
- (79) Lo, T. H. N.; Nguyen, M. V.; Tu, T. N. An Anchoring Strategy Leads to Enhanced Proton Conductivity in a New Metal-Organic Framework. *Inorg. Chem. Front.* **2017**, *4*, 1509–1516.
- (80) Nguyen, M. V.; Lo, T. H. N.; Luu, L. C.; Nguyen, H. T. T.; Tu, T. N. Enhancing Proton Conductivity in a Metal-Organic Framework at T > 80 °C by an Anchoring Strategy. *J. Mater. Chem. A* **2018**, *6*, 1816–1821.
- (81) Li, X. M.; Wang, Y. M.; Mu, Y. B.; Gao, J. K.; Zeng, L. Oriented Construction of Efficient Intrinsic Proton Transport Pathways in MOF-808. *J. Mater. Chem. A* **2022**, *10*, 18592–18597.
- (82) Sharma, A.; Lim, J.; Lee, S.; Han, S.; Seong, J.; Bin Baek, S.; Soo Lah, M. Superprotonic Conductivity of MOFs Confining Zwitterionic Sulfamic Acid as Proton Source and Conducting Medium. *Angew. Chem., Int. Ed.* **2023**, *62*, e202302376.
- (83) Sharma, A.; Lim, J.; Jeong, S.; Won, S.; Seong, J.; Lee, S.; Kim, Y. S.; Baek, S. B.; Lah, M. S. Superprotonic Conductivity of MOF-808 Achieved by Controlling the Binding Mode of Grafted Sulfamate. *Angew. Chem., Int. Ed.* **2021**, *60*, 14334–14338.
- (84) Zheng, S. L.; Wu, C. M.; Chung, L. H.; Zhou, H. Q.; Hu, J. Y.; Liu, Z. Q.; Wu, Y.; Yu, L.; He, J. Superprotonic Conductivity in Metal-Organic Frameworks by Charged-Layer-Mediated Proton Conduction. *ACS Energy Lett.* **2023**, *8*, 3095–3101.
- (85) Chen, G. L.; Ge, L.; Lee, J. H.; Zhu, Z. H.; Wang, H. Porous Coordination Polymer-Based Composite Membranes for High-Temperature Polymer Exchange Membrane Fuel Cells. *Matter* **2022**, *5*, 2031–2053.
- (86) Yu, X. H.; Bai, S. X.; Li, Q. Z.; Zhao, Z. Y.; Sun, Q.; Cao, S.; Cui, H. Z.; Liu, M. X.; Xu, Q.; Hou, C. C. Performance Optimization by Antioxidant Strategies for Proton Exchange Membrane Fuel Cells: Recent Progress and Future. *EnergyChem.* **2025**, *7*, 100142.
- (87) Zuo, P. P.; Li, Y. Y.; Wang, A. Q.; Tan, R.; Liu, Y. H.; Liang, X.; Sheng, F. M.; Tang, G. G.; Ge, L.; Wu, L.; Song, Q. L.; McKeown, N. B.; Yang, Z. J.; Xu, T. W. Sulfonated Microporous Polymer Membranes with Fast and Selective Ion Transport for Electrochemical Energy Conversion and Storage. *Angew. Chem., Int. Ed.* **2020**, *59*, 9564–9573.
- (88) Tzelepis, S.; Kavadias, K. A.; Marnellos, G. E.; Xydis, G. A Review Study on Proton Exchange Membrane Fuel Cell Electrochemical Performance Focusing on Anode and Cathode Catalyst Layer Modelling at Macroscopic Level. *Renewable Sustainable Energy Rev.* **2021**, *151*, 111543.
- (89) Feng, Y. B.; Dong, Z. M. Integrated Design and Control Optimization of Fuel Cell Hybrid Mining Truck with Minimized Lifecycle Cost. *Appl. Energy* **2020**, *270*, 115164.
- (90) Song, J. R.; Lan, T.; Wang, K. J.; Xie, Y. J.; Liu, D.; Wu, Y. L.; Li, W. J.; Wang, Z. Crystalline Poly (Ether Ether Ketone) Nanofiber-Reinforced Composite Proton Exchange Membranes with Dual Proton Channels. *J. Membr. Sci.* **2025**, *718*, 123702.
- (91) Wang, H.; Zhang, J. H.; Ning, X.; Tian, M. W.; Long, Y. Z.; Ramakrishna, S. Recent Advances in Designing and Tailoring Nanofiber Composite Electrolyte Membranes for High-Performance Proton Exchange Membrane Fuel Cells. *Int. J. Hydrogen Energy* **2021**, *46*, 25225–25251.
- (92) Ding, F.; Zou, T. T.; Wei, T.; Chen, L.; Qin, X. P.; Shao, Z. G.; Yang, J. J. The Pinhole Effect on Proton Exchange Membrane Fuel Cell (Pemfc) Current Density Distribution and Temperature Distribution. *Appl. Energy* **2023**, *342*, 121136.
- (93) Shabani, M.; Younesi, H.; Pontié, M.; Rahimpour, A.; Rahimejad, M.; Zinatizadeh, A. A. A Critical Review on Recent Proton Exchange Membranes Applied in Microbial Fuel Cells for Renewable Energy Recovery. *J. Cleaner Prod.* **2020**, *264*, 121446.
- (94) Si, G. R.; Yang, F.; He, T.; Kong, X. J.; Wu, W.; Li, T. C.; Wang, K. C.; Li, J. R. Enhancing Proton Conductivity in Zr-MOFs through Tuning Metal Cluster Connectivity. *J. Mater. Chem. A* **2022**, *10*, 1236–1240.
- (95) Patel, H. A.; Mansor, N.; Gadipelli, S.; Brett, D. J. L.; Guo, Z. X. Superacidity in Nafion/MOF Hybrid Membranes Retains Water at Low Humidity to Enhance Proton Conduction for Fuel Cells. *ACS Appl. Mater. Interfaces* **2016**, *8*, 30687–30691.
- (96) Wang, S. J.; Wahiduzzaman, M.; Davis, L.; Tissot, A.; Shepard, W.; Marrot, J.; Martineau-Corcus, C.; Hamdane, D.; Maurin, G.; Devautour-Vinot, S.; Serre, C. A Robust Zirconium Amino Acid Metal-Organic Framework for Proton Conduction. *Nat. Commun.* **2018**, *9*, 4937.
- (97) Meng, X.; Wang, H. N.; Song, S. Y.; Zhang, H. J. Proton-Conducting Crystalline Porous Materials. *Chem. Soc. Rev.* **2017**, *46*, 464–480.
- (98) Chen, X.; Li, G. Proton Conductive Zr-Based MOFs. *Inorg. Chem. Front.* **2020**, *7*, 3765–3784.
- (99) Zanchet, L.; da Trindade, L. G.; Bariviera, W.; Nobre Borba, K. M.; Santos, R. D. M.; Paganin, V. A.; de Oliveira, C. P.; Ticianelli, E. A.; Martini, E. M. A.; de Souza, M. O. Correction To: 3-Triethylammonium Propane Sulfonate Ionic Liquids for Nafion-Based Composite Membranes for Pem Fuel Cells. *J. Mater. Sci.* **2020**, *55*, 11794–11795.
- (100) Wu, B.; Lin, X. C.; Ge, L.; Wu, L.; Xu, T. W. A Novel Route for Preparing Highly Proton Conductive Membrane Materials with Metal-Organic Frameworks. *Chem. Commun.* **2013**, *49*, 143–145.

- (101) Yang, L. J.; Tang, B. B.; Wu, P. Y. Metal-Organic Framework-Graphene Oxide Composites: A Facile Method to Highly Improve the Proton Conductivity of Pems Operated under Low Humidity. *J. Mater. Chem. A* **2015**, *3*, 15838–15842.
- (102) Dong, X.-Y.; Wang, J.-H.; Liu, S.-S.; Han, Z.; Tang, Q.-J.; Li, F.-F.; Zang, S.-Q. Synergy between Isomorphous Acid and Basic Metal-Organic Frameworks for Anhydrous Proton Conduction of Low-Cost Hybrid Membranes at High Temperatures. *ACS Appl. Mater. Interfaces* **2018**, *10*, 38209–38216.
- (103) Feng, K.; Meng, L.; Xu, J.; Zhao, P.; Li, N.; Lei, J. Introduction of Bifunctionalized UiO-66-NH<sub>2</sub> for Highly Conductive and Long-Term Stable Fluorene-Based Sulfonated Poly(Aryl Ether Ketone Sulfone) Pems. *ACS Applied Polymer Materials* **2024**, *6*, 10916–10926.
- (104) Wang, S.; Yan, G.; Kang, X.; Li, Z.; Zhuang, X. Bio-Metal Organic Framework Functionalized Nanofibers as Efficient Proton-Conducting for Proton Exchange Membrane. *Int. J. Hydrogen Energy* **2024**, *87*, 1347–1355.
- (105) Wang, L. L.; Wen, Q.; Jia, P.; Jia, M. J.; Lu, D. N.; Sun, X. M.; Jiang, L.; Guo, W. Light-Driven Active Proton Transport through Photoacid- and Photobase-Doped Janus Graphene Oxide Membranes. *Adv. Mater.* **2019**, *31*, 1903029.
- (106) Kaur, D.; Khaniya, U.; Zhang, Y.; Gunner, M. R. Protein Motifs for Proton Transfers That Build the Transmembrane Proton Gradient. *Front. Chem.* **2021**, *9*, 660954.
- (107) Xiang, F. H.; Chen, S. M.; Yuan, Z.; Li, L.; Fan, Z. W.; Yao, Z. Z.; Liu, C. L.; Xiang, S. C.; Zhang, Z. J. Switched Proton Conduction in Metal-Organic Frameworks. *JACS Au* **2022**, *2*, 1043–1053.
- (108) Bigdeli, F.; Lollar, C. T.; Morsali, A.; Zhou, H. C. Switching in Metal-Organic Frameworks. *Angew. Chem., Int. Ed.* **2020**, *59*, 4652–4669.
- (109) Zhou, Z. X.; Vázquez-González, M.; Willner, I. Stimuli-Responsive Metal-Organic Framework Nanoparticles for Controlled Drug Delivery and Medical Applications. *Chem. Soc. Rev.* **2021**, *50*, 4541–4563.
- (110) Grzelczak, M.; Liz-Marzán, L. M.; Klajn, R. Stimuli-Responsive Self-Assembly of Nanoparticles. *Chem. Soc. Rev.* **2019**, *48*, 1342–1361.
- (111) Müller, K.; Helfferich, J.; Zhao, F. L.; Verma, R.; Kanj, A. B.; Meded, V.; Bléger, D.; Wenzel, W.; Heinke, L. Switching the Proton Conduction in Nanoporous, Crystalline Materials by Light. *Adv. Mater.* **2018**, *30*, 1706551.
- (112) Guo, W.; Tian, Y.; Jiang, L. Asymmetric Ion Transport through Ion-Channel-Mimetic Solid-State Nanopores. *Acc. Chem. Res.* **2013**, *46*, 2834–2846.
- (113) Jochum, F. D.; Theato, P. Temperature- and Light-Responsive Smart Polymer Materials. *Chem. Soc. Rev.* **2013**, *42*, 7468–7483.
- (114) Nagarkar, S. S.; Horike, S.; Itakura, T.; Le Ouay, B.; Demessence, A.; Tsujimoto, M.; Kitagawa, S. Enhanced and Optically Switchable Proton Conductivity in a Melting Coordination Polymer Crystal. *Angew. Chem., Int. Ed.* **2017**, *56*, 4976–4981.
- (115) Liu, Z. Y.; Zhang, H.; Ren, X. Y.; Luo, H. B.; Zhang, J.; Ren, X. M. Functionalization of Cluster-Nodes in a Metal-Organic Framework for Light-Manipulating Proton Conduction. *ACS Mater. Lett.* **2024**, *6*, 461–465.
- (116) Kanj, A. B.; Chandresh, A.; Gerwien, A.; Grosjean, S.; Bräse, S.; Wang, Y.; Dube, H.; Heinke, L. Proton-Conduction Photomodulation in Spiropyran-Functionalized MOFs with Large on-off Ratio. *Chem. Sci.* **2020**, *11*, 1404–1410.
- (117) Liang, H.-Q.; Guo, Y.; Shi, Y.; Peng, X.; Liang, B.; Chen, B. A Light-Responsive Metal-Organic Framework Hybrid Membrane with High on/off Photoswitchable Proton Conductivity. *Angew. Chem., Int. Ed.* **2020**, *59*, 7732–7737.
- (118) Fan, S.; Wang, S.; Wang, X.; Li, Z.; Ma, X.; Wan, X.; Hussain, S.; Peng, X. Photogated Proton Conductivity of ZIF-8 Membranes Co-Modified with Graphene Quantum Dots and Polystyrene Sulfonate. *Science China Materials* **2021**, *64*, 1997–2007.
- (119) Li, P.; Li, Z.; Guo, Y.; Deng, Z.; Wang, X.; Ma, X.; Peng, X. Ag-DNA@ZIF-8 Membrane: A Proton Conductive Photoswitch. *Appl. Mater. Today* **2020**, *20*, 100761.
- (120) Lu, N.; Gao, X. Q.; Yang, C.; Xiao, F.; Wang, J. D.; Su, X. T. Enhanced Formic Acid Gas-Sensing Property of WO<sub>3</sub> Nanorod Bundles Via Hydrothermal Method. *Sens. Actuators, B* **2016**, *223*, 743–749.
- (121) Wu, Y.; Hua, C. X.; Liu, Z. S.; Yang, J. L.; Huang, R. R.; Li, M.; Liu, K. Q.; Miao, R.; Fang, Y. High-Performance Sensing of Formic Acid Vapor Enabled by a Newly Developed Nanofilm-Based Fluorescent Sensor. *Anal. Chem.* **2021**, *93*, 7094–7101.
- (122) Huang, S. C.; Cheng, C. C.; Lai, Y. H.; Lin, C. Y. Sustainable and Selective Formic Acid Production from Photoelectrochemical Methanol Reforming at near-Neutral pH Using Nanoporous Nickel-Iron Oxyhydroxide-Borate as the Electrocatalyst. *Chem. Eng. J.* **2020**, *395*, 125176.
- (123) Rice, C.; Ha, S.; Masel, R. I.; Waszczuk, P.; Wieckowski, A.; Barnard, T. Direct Formic Acid Fuel Cells. *J. Power Sources* **2002**, *111*, 83–89.
- (124) Ricke, S. C.; Dittoe, D. K.; Richardson, K. E. Formic Acid as an Antimicrobial for Poultry Production: A Review. *Front. Vet. Sci.* **2020**, *7*, 563.
- (125) Liu, R. L.; Qu, W. T.; Dou, B. H.; Li, Z. F.; Li, G. Proton-Conductive 3d Lniii Metal-Organic Frameworks for Formic Acid Impedance Sensing. *Chem.—Asian J.* **2020**, *15*, 182–190.
- (126) Liesivuori, J.; Savolainen, A. H. Methanol and Formic Acid Toxicity: Biochemical Mechanisms. *Pharmacol. Toxicol.* **1991**, *69*, 157–163.
- (127) Ueta, I.; Nakamura, Y.; Kawakubo, S.; Saito, Y. Determination of Aqueous Formic and Acetic Acids by Purge-and-Trap Analysis with a Needle-Type Extraction Device and Gas Chromatography Barrier Discharge Ionization Detector. *Anal. Sci.* **2018**, *34*, 201–205.
- (128) Zhou, D. D.; Hou, Q. X.; Liu, W.; Ren, X. L. Rapid Determination of Formic and Acetic Acids in Biomass Hydrolysate by Headspace Gas Chromatography. *J. Ind. Eng. Chem.* **2017**, *47*, 281–287.
- (129) Zhu, W.; Song, H. J.; Lv, Y. Triazine-Based Graphitic Carbon Nitride: Controllable Synthesis and Enhanced Cataluminescent Sensing for Formic Acid. *Anal. Bioanal. Chem.* **2018**, *410*, 7499–7509.
- (130) Mori, K.; Dojo, M.; Yamashita, H. Pd and Pd-Ag Nanoparticles within a Macroporous Basic Resin: An Efficient Catalyst for Hydrogen Production from Formic Acid Decomposition. *ACS Catal.* **2013**, *3*, 1114–1119.
- (131) Genovese, M. E.; Colusso, E.; Colombo, M.; Martucci, A.; Athanassiou, A.; Fragouli, D. Acidochromic Fibrous Polymer Composites for Rapid Gas Detection. *J. Mater. Chem. A* **2017**, *5*, 339–348.
- (132) Sandström, K. J. M.; Newman, J.; Sunesson, A.-L.; Levin, J.-O.; Turner, A. P. F. Amperometric Biosensor for Formic Acid in Air. *Sens. Actuators, B* **2000**, *70*, 182–187.
- (133) Chen, G. L.; Li, J.; Meng, F. L. Formic Acid Gas Sensor Based on Coreless Optical Fiber Coated by Molybdenum Disulfide Nanosheet. *J. Alloys Compd.* **2022**, *896*, 163063.
- (134) Lin, F. R.; Liu, Z. Y.; Zhang, H.; Liu, M.; Luo, H. B.; Zou, Y.; Ren, X. M. Proton Conductive Thin Films of Metal-Organic Framework for Impedance Detection of Formic Acid. *Microporous Mesoporous Mater.* **2023**, *360*, 112722.
- (135) Liang, H. Q.; Guo, Y.; Peng, X. S.; Chen, B. L. Light-Gated Cation-Selective Transport in Metal-Organic Framework Membranes. *J. Mater. Chem. A* **2020**, *8*, 11399–11405.
- (136) Qian, T. Y.; Zhang, H. C.; Li, X. Y.; Hou, J.; Zhao, C.; Gu, Q. F.; Wang, H. T. Efficient Gating of Ion Transport in Three-Dimensional Metal-Organic Framework Sub-Nanochannels with Confined Light-Responsive Azobenzene Molecules. *Angew. Chem., Int. Ed.* **2020**, *59*, 13051–13056.
- (137) Hou, J.; Zhao, C.; Zhang, H. C. Bio-Inspired Subnanofluidics: Advanced Fabrication and Functionalization. *Small Methods* **2024**, *8*, 2300278.

- (138) Daniel, M.; Mathew, G.; Anpo, M.; Neppolian, B. MOF Based Electrochemical Sensors for the Detection of Physiologically Relevant Biomolecules: An Overview. *Coord. Chem. Rev.* **2022**, *468*, 214627.
- (139) Ye, T. T.; Wang, X. T.; Wang, L.; Ren, S. N.; Yang, L. N.; Chen, L. H. Novel Electrochemical Sensor Based on One-Step Encapsulation of Metal-Organic Framework (MOF) for Simultaneous Detection of Sars-Cov and Sars-Cov-2. *ACS Appl. Mater. Interfaces* **2024**, *16*, 59648–59661.
- (140) Zhang, L.; Han, Y.; Sun, M.; Li, S. B. Non-Enzymatic Electrochemical Sensor Based on Ionic Liquid [BMIM][PF<sub>6</sub>] Functionalized Zirconium-Copper Bimetallic MOF Composite for the Detection of Nitrite in Food Samples. *Food Chem.* **2024**, *456*, 140023.
- (141) Ladhi, R.; Dhillon, A. K.; Singh, M. Ultrathin MOF Nanosheets and Their Mixed-Matrix Membranes for Ammonia and Aliphatic Amine Sensing in Water. *Nanoscale* **2024**, *16*, 8836–8842.
- (142) Sharma, S.; Dutta, S.; Dam, G. K.; Ghosh, S. K. Neutral Nitrogen Donor Ligand-Based MOFs for Sensing Applications. *Chem.—Asian J.* **2021**, *16*, 2569–2587.
- (143) Vikrant, K.; Kumar, V.; Ok, Y. S.; Kim, K.-H.; Deep, A. Metal-Organic Framework (MOF)-Based Advanced Sensing Platforms for the Detection of Hydrogen Sulfide. *TrAC, Trends Anal. Chem.* **2018**, *105*, 263–281.
- (144) Li, C. M.; Huang, J. P.; Zhu, H. L.; Liu, L. L.; Feng, Y. M.; Hu, G.; Yu, X. B. Dual-Emitting Fluorescence of Eu/Zr-MOF for Ratiometric Sensing Formaldehyde. *Sens. Actuators, B* **2017**, *253*, 275–282.
- (145) Liu, R. L.; Shi, Z. Q.; Wang, X. Y.; Li, Z. F.; Li, G. Two Highly Stable Proton Conductive Cobalt(II)-Organic Frameworks as Impedance Sensors for Formic Acid. *Chem.—Eur. J.* **2019**, *25*, 14108–14116.
- (146) Liu, M.; Zhang, J.; Kong, Y. R.; Luo, H. B.; Liu, Y. Y.; Ren, X. M. Thin Films of an Ultrastable Metal-Organic Framework for Formic Acid Sensing with High Selectivity and Excellent Reproducibility. *ACS Mater. Lett.* **2021**, *3*, 1746–1751.
- (147) Tammanoon, N.; Wisitsoraat, A.; Tuantranont, A.; Liewhiran, C. Flame-Made Zn-Substituted SnO<sub>2</sub> Nanoparticulate Compound for Ultra-Sensitive Formic Acid Gas Sensing. *J. Alloys Compd.* **2021**, *871*, 159547.
- (148) Lin, F. R.; Liu, Z. Y.; Zhang, H.; Liu, M.; Luo, H. B.; Zou, Y.; Ren, X. M. Proton Conductive Thin Films of Metal-Organic Framework for Impedance Detection of Formic Acid. *Microporous Mesoporous Mater.* **2023**, *360*, 112722.